We are IntechOpen,
the world's leading publisher of
Open Access books
Built by scientists, for scientists

4,800
Open access books available

122,000
International authors and editors

135M
Downloads

Our authors are among the

154
Countries delivered to

TOP 1%
most cited scientists

12.2%
Contributors from top 500 universities

CLARIVATE ANALYTICS

BOOK
CITATION
INDEX

INDEXED

WEB OF SCIENCE™

Selection of our books indexed in the Book Citation Index
in Web of Science™ Core Collection (BKCI)

Interested in publishing with us?
Contact book.department@intechopen.com

Numbers displayed above are based on latest data collected.
For more information visit www.intechopen.com

Nanograin Formation within Shear Bands in Cold-Rolled Titanium

Dengke Yang and Huimin Yang

Additional information is available at the end of the chapter

Abstract

Microstructure evolution within the shear localization areas in a commercial titanium plate subjected to cold rolling was systematically investigated. A shear band with a width of approximately 25 μm was formed. The microstructure inside the shear band was mainly equiaxed nanograins with an average size of 70 nm. Transmission electron microscopy (TEM) observations revealed that the grain refinement inside the shear band was completely via a shear deformation-induced splitting and breakdown twin lamella process, instead of a nucleation and growth of new grains. The shear localization starts with the formation and multiplication of mechanical twins, which leads to the development of a twin/matrix lamellar structure aligned along the shear direction. The twin/matrix lamellae subsequently undergo gradual splitting and transverse breakdown, giving rise to fine elongated subgrains. The continuing lath breakdown, in combination with grain lateral sliding and lattice rotations, ultimately leads to the formation of a mix of roughly equiaxed, nanosized (sub)grains within the center of macroscopic shear band at large strains.

Keywords: nanograin, shear band, titanium, cold rolling, grain refining mechanism

1. Introduction

Shear band is a highly localized deformation mode that usually develops in a majority of metallic materials subjected to heavy loading, which generally leads to their limited applicability and high susceptibility to catastrophic failure in load-bearing applications [1, 2]. In the past two decades, the residual microstructures within shear bands have been studied at large using transmission electron microscopy, facilitated by the band convenient location in a restricted area of the hat-shaped specimens used in dynamic impact experiments [3–16]. These shear bands are

frequently termed "adiabatic" shear bands, as they usually experience very high levels of strain rate, and the shear localization is frequently considered to be adiabatic with large temperature increases inside the bands [17]. The microstructures within adiabatic shear bands often undergo subsequent modifications through the recovery, recrystallization and phase transformation processes, which generally contribute to significant microstructure refinement through the formation of (sub)grains/fragments with the size of several tens of nanometers [1, 10].

The shear bands occurring in metals deformed by rolling and other quasi-static deformation modes [18–27] generally display microstructural features that markedly differ from those observed within their adiabatic counterparts. Strong texturing as well as elongated and heavily dislocated grains within the shear bands in a consolidated ultrafine-grained iron subjected to quasi-static compression has been revealed [27], which is strikingly different from the microstructure commonly found in the center of adiabatic shear bands. Refs. [18, 28, 29] performed detailed investigations, using a combination of the electron backscattering diffraction (EBSD) in a scanning electron microscope and the transmission electron microscopy (TEM) techniques, on the evolution of relatively coarse and/or well-recovered microstructures within shear bands formed during rolling or plane strain compression. At present, however, such investigations on the microstructures with extremely fine grains and high dislocation densities produced by heavy rolling deformation at room temperature are rather scarce and significantly less detailed. Such investigation is thus rather difficult and requires the time-consuming TEM technique. Furthermore, the rather random distribution of these bands within the matrix also causes the difficulty in preparation of targeted TEM specimens. The scale and character of the microstructures observed inside these shear bands have been found to share some similarity to those observed in ultrafine-grained materials processed by severe plastic deformation (SPD) [1, 30]. The microstructure refining mechanisms operating within the shear bands subjected to heavy rolling deformation will help to the better understand the grain-refining mechanisms occurring in other SPD processes. Nevertheless, deformation mechanisms themselves have frequently been able to achieve a significant refinement of the adiabatic shear band microstructure, in particular when these mechanisms involved mechanical twinning.

Apart from dislocation slip processes, mechanical twinning plays an important role in plastic deformation of hexagonal close packed (HCP) structure metals that have a limited number of slip systems. The predominant twinning systems are $\{10\bar{1}2\}\langle10\bar{1}\bar{1}\rangle$ tensile twins and $\{11\bar{2}2\}\langle11\bar{2}\bar{3}\rangle$ compression twins during deformation of hcp titanium at ambient temperature, accommodating extension and contraction along the c-axis, respectively [31, 32]. The intersection of twins and the formation of secondary and tertiary twins result in progressive grain refinement. At relatively modest strains, a gradual decrease in twin activity and saturation in twinning ultimately have been achieved, causing dislocation slip to dominate the deformation process at high strains [32–35]. The extremely fine, roughly equiaxed grains with a mean size of 80–100 nm in commercial purity titanium subjected to accumulated roll bonding has been reported [36]. These grains might possibly initiate from macro-shear and micro-shear bands, but details of their formation mechanism still remain to be elucidated.

This chapter will review our work on the nanograin formation in a cold-rolled titanium and supplement and update the extensive article published by our group. We performed a

detailed TEM study on the microstructure evolution within the shear bands in commercial purity titanium subjected to heavy cold rolling and focus on elucidating the microstructure-refining mechanisms within the shear bands.

2. Experimental procedures

A titanium plate with a mean grain size of about 60 μm was cold rolled from 12 to 2 mm in thickness with a per pass reduction of 16.7% at a strain rate of 3 s^{-1}. The von Mises equivalent strains corresponding to different rolling reductions were calculated by $\varepsilon_{VM} = \frac{-2}{\sqrt{3}}\ln\left(\frac{t}{t_0}\right)$, with t_0 and t being the plate thickness before and after rolling, respectively. The shear strain accumulated within the shear bands was estimated using the method introduced by Ref. [9]. The microstructure both outside and within the shear localization areas was investigated by scanning electron microscopy (SEM) and TEM. An SEM study was carried out using a Zeiss Supra 55VP field-emission gun microscope operated at 10 kV. TEM investigation was performed using a Jeol JEM 2100 LaB$_6$ microscope operated at 200 kV. The observation sections were perpendicular to the transverse direction (TD) of the rolled plate. The etching of the samples was carried out using a solution composed of 50 ml H$_2$O, 40 ml HNO$_3$, and 10 ml HF.

The TEM samples are prepared as follows. A slice of the rolled specimen was first cut perpendicular to TD. In order to locate the shear bands, one side of the slice was metallographically polished and etched, then a light scratch was used to mark the shear band location and the rolling direction. The sample slice was then thinned by grinding from the opposite side to a sheet with thickness of approximately 100 μm. A disc with a diameter of 3 mm was subsequently
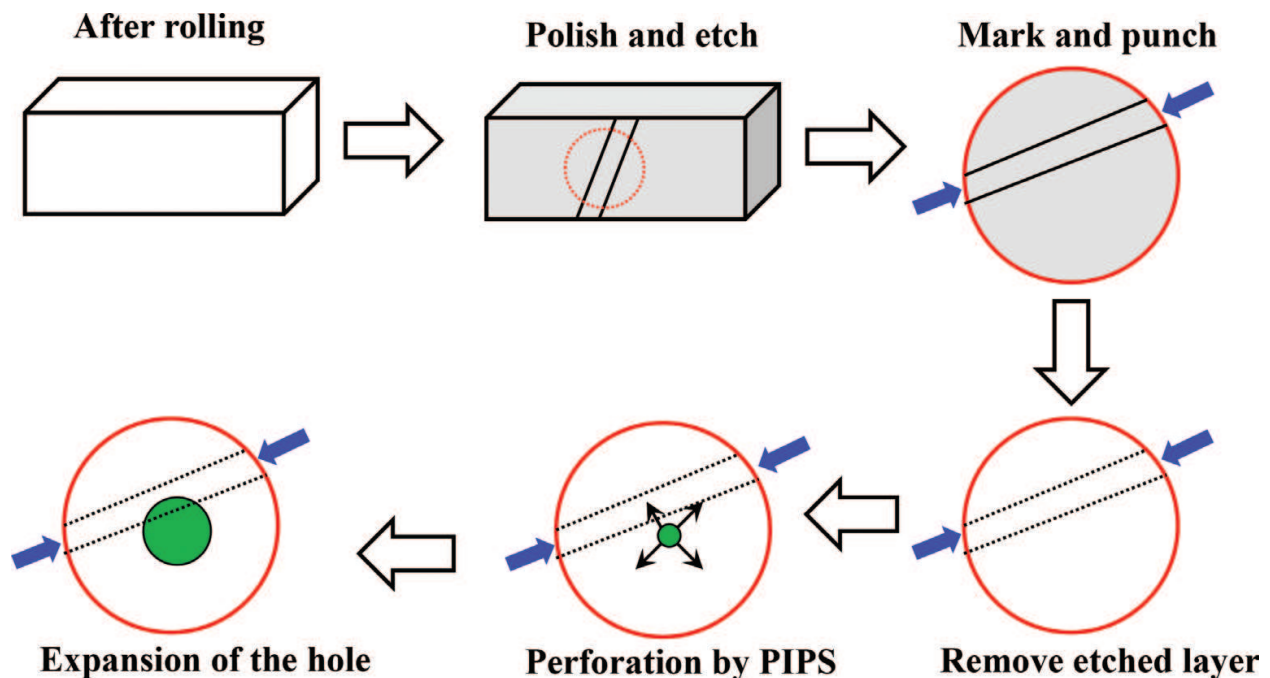

Figure 1. Schematic illustration of the preparation process for the TEM samples.

punched out from the sheet, ensuring that the intersection of the two marker lines was located close to the center of the disc, and the rolling direction was marked through a pair of fine notches placed on the disc rim. The disc was then carefully ground to approximately 50 μm in thickness and finally subjected to perforation using a low-energy ion milling in a Gatan PIPS system. **Figure 1** is a schematic illustration of the process for the preparation of TEM specimen.

3. Results

3.1. SEM observation of shear localization

Figure 2 shows that the micro-regions with localized shear were first initiated close to the edge of the rolled plate at von Mises equivalent strains (εVM) of 0.47 (rolling reduction of 33%) (**Figure 2a**). The S-like flow lines were extensively stretched in these micro-regions. The surrounding elongated grains, however, contained extensive deformation twinning, as shown in **Figure 3**. After 50% rolling reduction (εVM = 0.80), a localized microscopic shear band, having a width of approximately 8 μm and being inclined at an angle of about 40°relative to the rolling direction, was formed (**Figure 2b**); the deformation twins and the stretched grain boundaries located at the shear band boundaries gradually bent in a curve appearance when
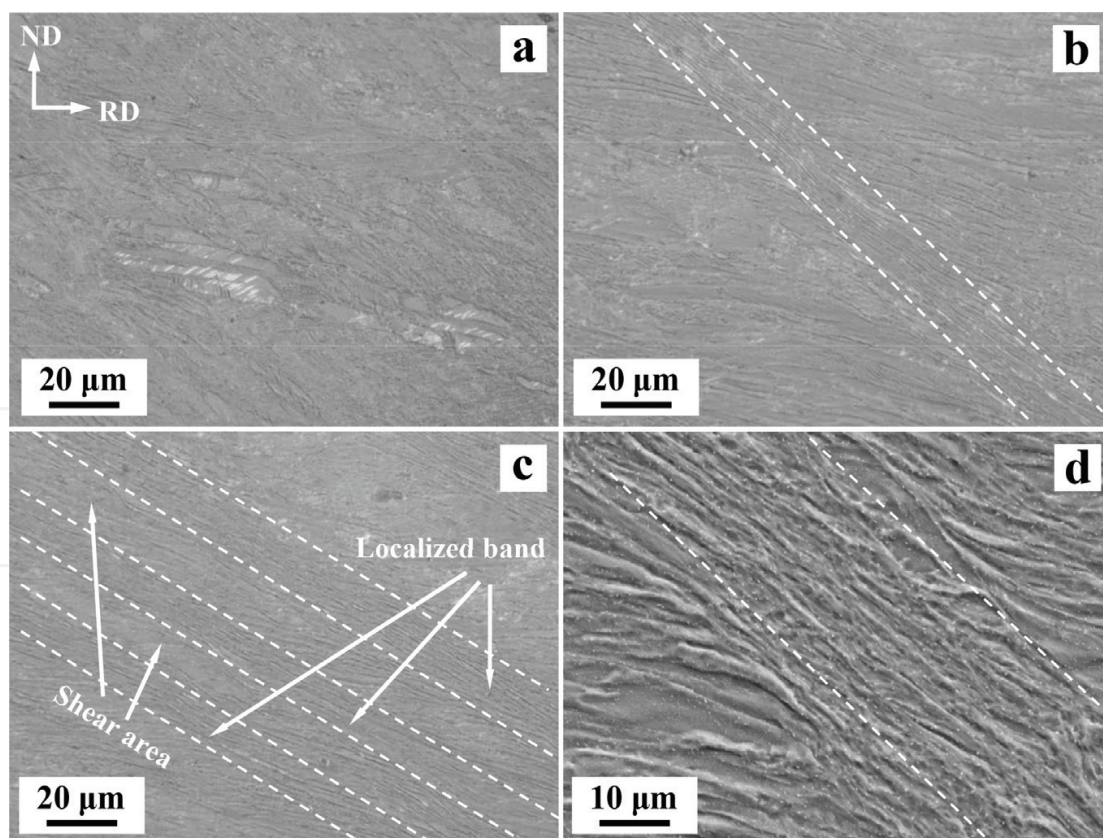

Figure 2. SEM micrographs showing the shear bands (delineated by dashed lines) developed at different rolling reductions: (a) 33% (εVM = 0.47), (b) 50% (εVM = 0.80), (c) 67% (εVM = 1.27), and (d) 83% (εVM = 2.07). RD and ND indicate the rolling and normal directions, respectively.
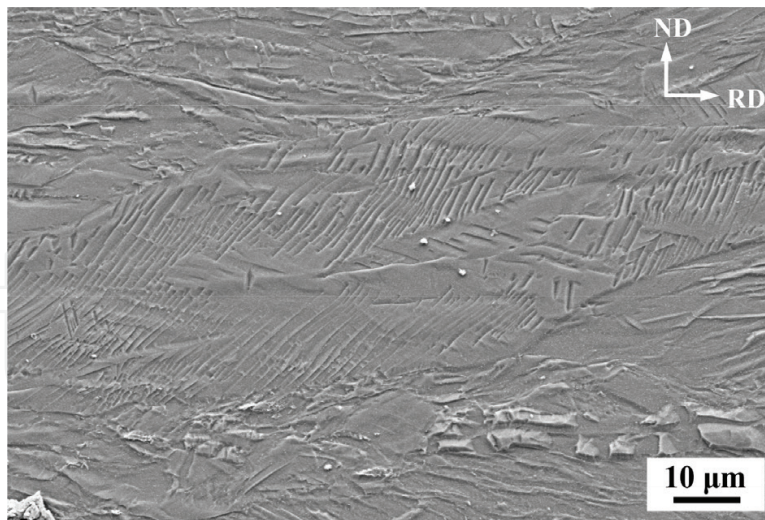
Figure 3. SEM micrograph showing extensive deformation twinning within the deformed grains at 33% rolling reduction (εVM = 0.47).

merging into the band. At the rolling reduction of 67% (εVM = 1.27), several microscopic shear bands formed and widened by expensing the adjacent deformed matrix regions (**Figure 2c**). When the rolling reduction reached 83% (εVM = 2.07), a well-developed macroscopic shear band having a width of about 25 μm was formed and the entire sheared region was filled with parallel flow lines (**Figure 2d**).

3.2. TEM quantification of the microstructure within shear bands

After 33% rolling reduction, the sheared micro-regions showed a significantly finer substructure than the surrounding matrix (**Figure 4a**). The selected area diffraction (SAD) patterns obtained from the micro-regions (inset in **Figure 4b**) indicated the occurrence of large-angle misorientation fragments. The neighboring matrix mainly consisted of dislocation cells separated by low-angle boundaries with a significant dislocation density in the interior. The corresponding SAD patterns (the inset in **Figure 4a**) were close to those typically obtained for single crystals. The sheared micro-regions contained fine twin/matrix lamellae, thin laths and elongated subgrain structures interspersed with the deformed matrix comprising dislocation cells. The elongated subgrains, however, could not be clearly resolved due to a high density of dislocations (**Figure 4b**).

When increased to 50% rolling reduction, a localized microscopic shear band contained regions of thin lamellae/laths interspersed with fine elongated subgrains (**Figure 5a**). **Figure 5b** shows that fine elongated subgrains contained lower dislocation density in the interior which are more evident than those formed at 33% rolling reduction. The histogram presented in **Figure 5c** shows a rather broad subgrain size distribution of 20–240 nm with a mean value of about 110 nm. Statistical determination of the subgrain longitudinal (d_L) and transverse length (d_T) revealed that the average d_L/d_T ratio was about 2.5 (inset in **Figure 5c**). Statistical evaluation of θ, the angle between the subgrain elongation axis and the rolling direction (RD), has an average value of around 40°, indicating a strong morphological texture with most of the subgrains retaining their elongation axis parallel to the shear direction (**Figure 5d**).
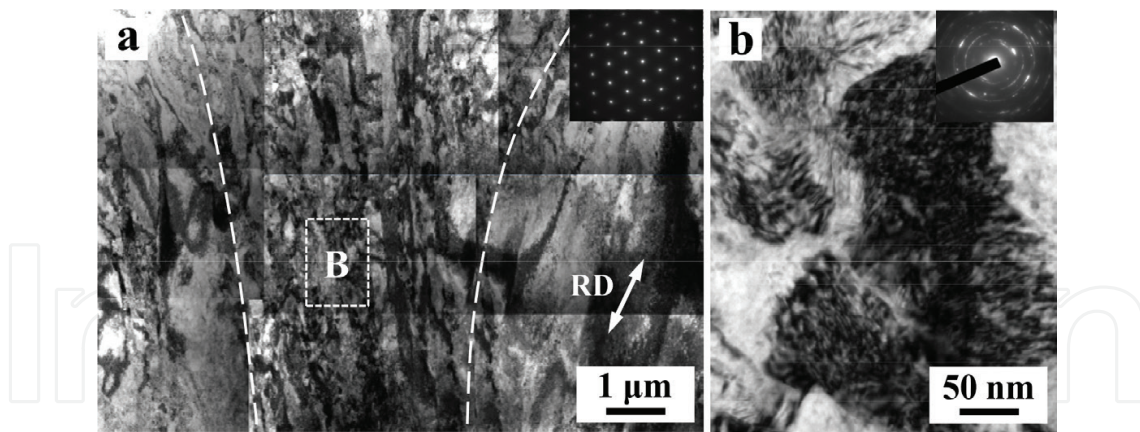
Figure 4. TEM micrographs obtained after 33% rolling reduction (εVM = 0.47): (a) bright-field image of a sheared micro-region (delineated by dashed lines) and the matrix. The inset shows the matrix SAD pattern and RD indicates the rolling direction; (b) high-magnification bright-field image of the sheared micro-region area marked in (a) (the inset shows the corresponding SAD pattern).
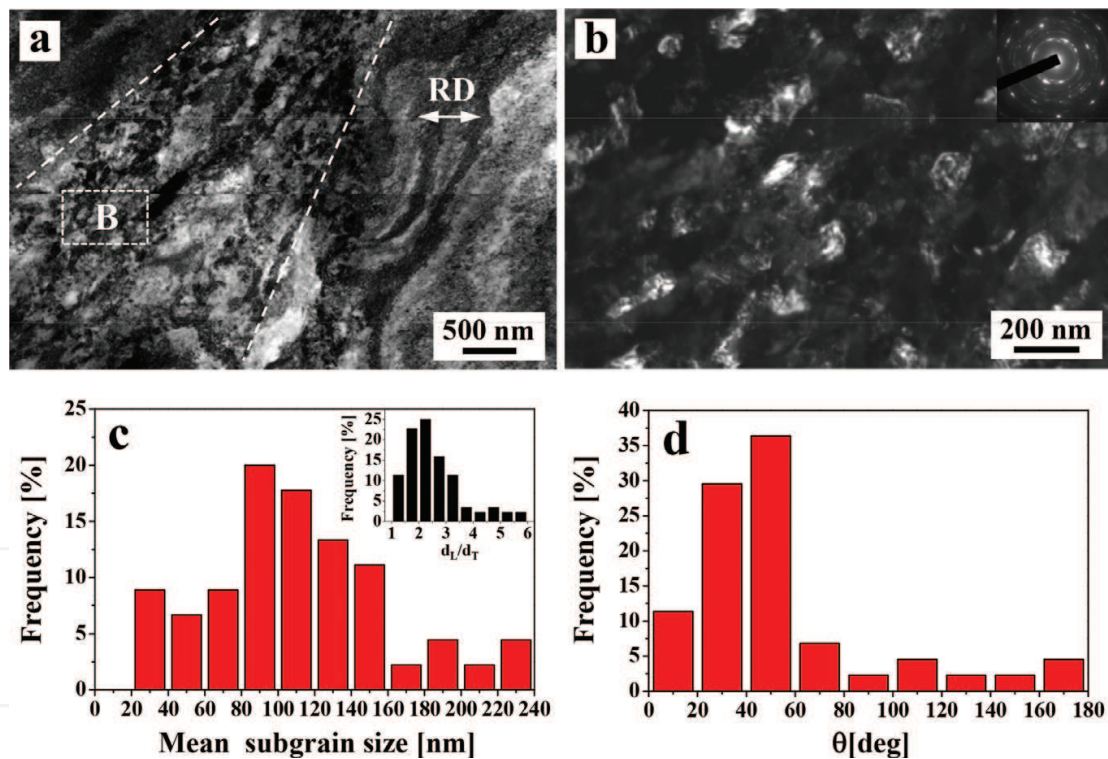

Figure 5. TEM micrographs obtained after 50% rolling reduction (εVM = 0.80): (a) bright-field image of a region containing the localized microscopic shear band delineated by dashed lines. RD indicates the rolling direction; (b) dark-field image of the shear band area marked in (a) (the inset shows the corresponding SAD pattern); (c) subgrain size distribution for the microscopic shear band (the inset shows the corresponding histogram of dL/dT ratios); (d) distribution of the angles between the subgrain elongation axes and RD.

At 67% rolling reduction, the microstructure inside the localized microscopic shear bands became more homogeneous but maintained its alignment parallel to the shear direction (**Figure 6a**). The very fine, elongated rectangular or elliptical subgrains were observed (**Figure 6b** and **c**).

The SAD pattern of the corresponding area (inset in **Figure 6c**) exhibits diffuse arcing spots indicating large misorientations between adjacent subgrains. **Figure 6d** shows the histogram, indicating that most of the subgrains had a size in the range of 20–200 nm with a mean value of about 90 nm. The corresponding average value of the d_L/d_T ratio was about 2.0 (inset in **Figure 6d**). The distribution of θ (**Figure 6e**) indicates that the fine subgrains had a more random morphological alignment than those at 50% reduction.
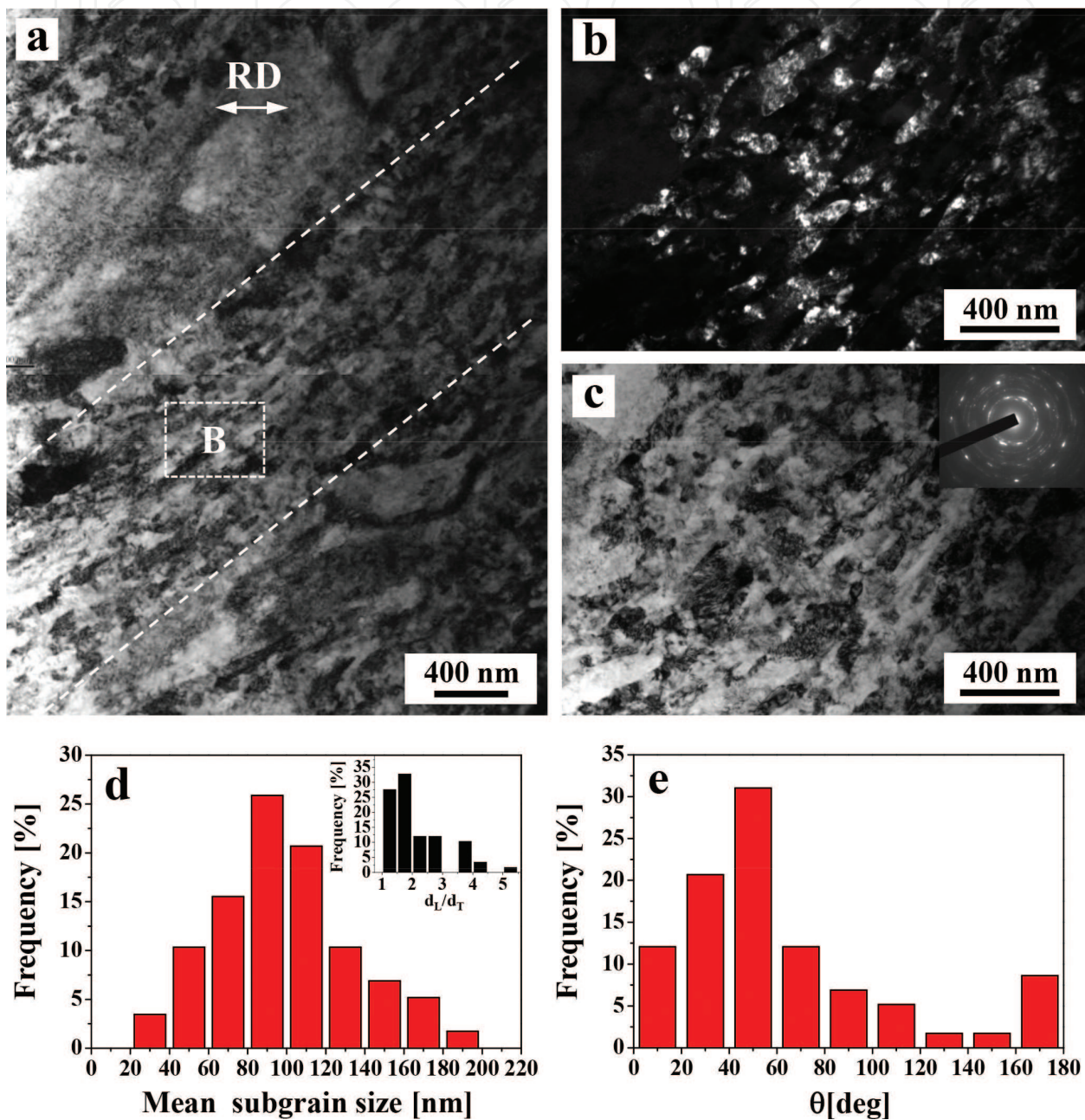

Figure 6. TEM micrographs obtained after 67% rolling reduction: (εVM = 1.27) (a) bright-field image of a region containing the localized microscopic shear band delineated by dashed lines. RD indicates the rolling direction; (b) dark-field image of the subgrains in the shear band area marked in (a); (c) bright-field image of the same area (the inset shows the corresponding SAD pattern); (d) subgrain size distribution for the microscopic shear band (the inset shows the corresponding histogram of dL/dT ratios); (e) distribution of the angles between the subgrain elongation axes and RD.
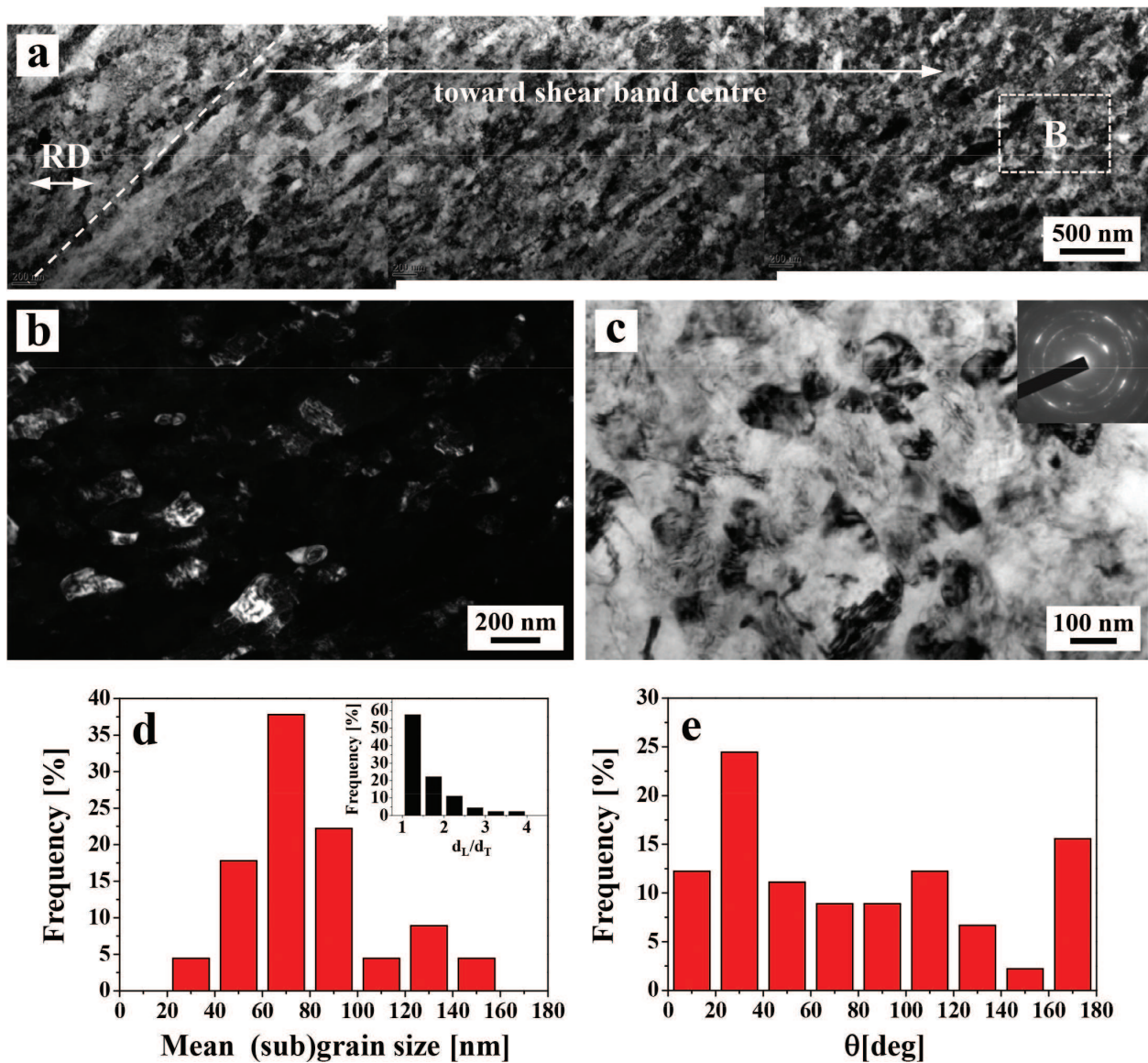
Figure 7. TEM micrographs obtained after 83% rolling reduction (εVM = 2.07): (a) bright-field image of a part of the macroscopic shear band with its boundary marked by a dashed line. RD indicates the rolling direction; (b) dark-field image of the nanosized (sub)grains present in the shear band central region indicated in (a); (c) bright-field image of the same area (the inset shows the corresponding SAD pattern); (d) (sub)grain size distribution for the macroscopic shear band center (the inset shows the corresponding histogram of d_L/d_T ratios); (e) distribution of the angles between the (sub) grain elongation axes and RD.

When the rolling reduction increased to 83%, two distinct regions developed within the macroscopic shear band. Wide outer regions were mainly filled with fine elongated subgrains, whereas the shear band center was occupied by roughly equiaxed nanosized (sub)grains (**Figure 7a**). These ultrafine (sub)grains showed no trace of the shear direction (**Figure 7b** and **c**). Some of these (sub)grains appeared to contain few dislocations and were delineated by rather sharp boundaries. **Figure 7d** reveals that the (sub)grains possessed a size range from 20 to 160 nm and had a mean size of about 70 nm. The corresponding average value of the d_L/d_T ratio was approximately 1.2 (inset in **Figure 7d**), clearly showing that these nanosized (sub) grains were mostly roughly equiaxed. The distribution of θ became randomized (**Figure 7e**), indicating the non-contiguous nature of these nanosized (sub)grains.

3.3. The microstructure refinement mechanisms within shear bands

The boundary regions between the shear localization areas and the matrix, as well as the outer regions of the localized bands, provided important information of the mechanism of micro-structure evolution within the shear bands. **Figure 8** shows the mechanical twin in the boundary between a sheared micro-region and the matrix at 33% rolling reduction. The twin lamella consisted of several segments, three of which are labeled T_1, T_2 and T_3 in **Figure 8a**. It should be noted that the TEM foil was tilted so that the twin boundary displayed a minimum projected width and thus was in the "edge-on" position. The SAD patterns for the surrounding matrix (**Figure 8b**) and the main part of the twin lamella T_1 (**Figure 8c**) were both close to the $[1\bar{2}10]$ zone axis. The precise zone axes for the matrix and twin were reached at slightly different foil tilts by about 2°. These patterns shared a coincidental $(10\bar{1}2)$ reflection (circled in **Figure 8b** and **c**) and the corresponding diffraction spots displayed mirror symmetry with respect to a common $(10\bar{1}2)$ plane, which was approximately parallel to the twin planes (**Figure 8d**). This indicates that the twin segment T_1 represented a fine $\{10\bar{1}2\}\langle 10\bar{1}\bar{1}\rangle$ tensile twin, which was further
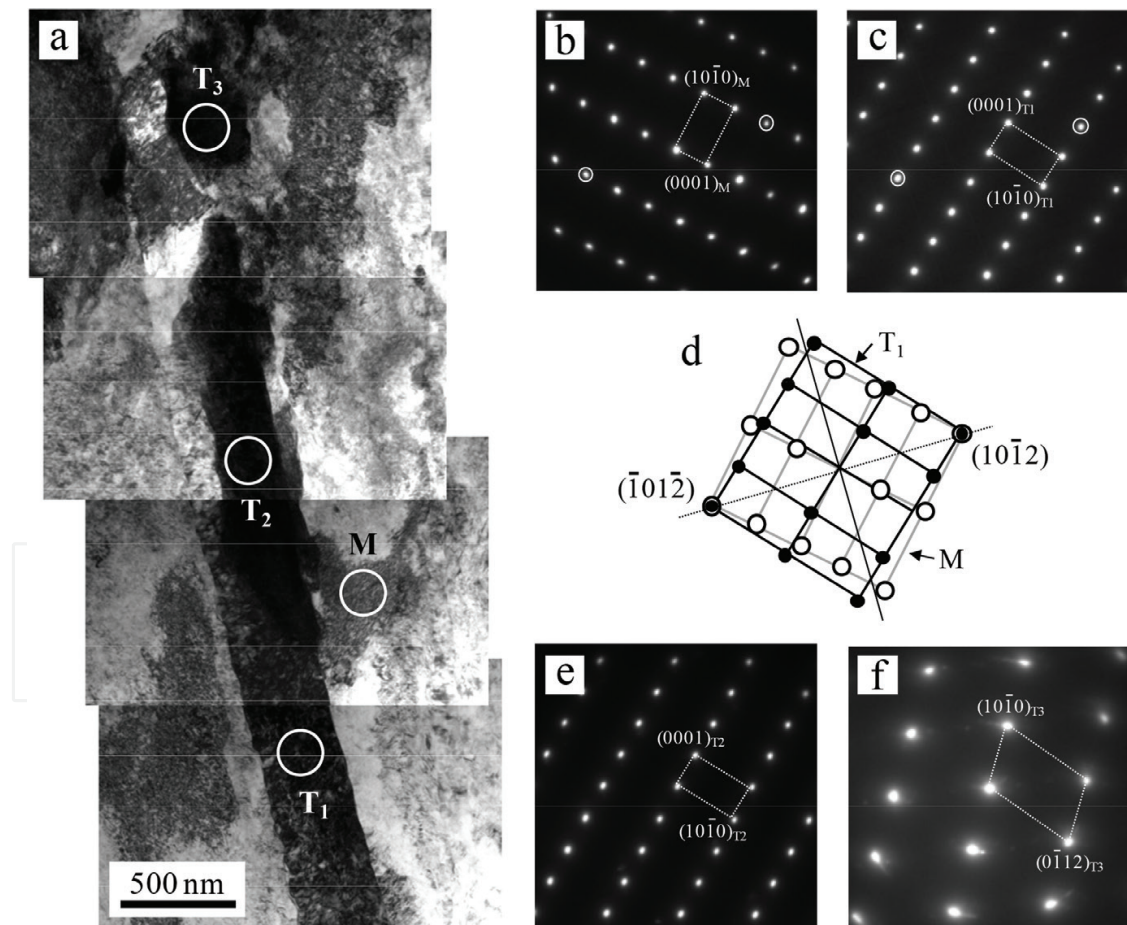

Figure 8. TEM analysis of a mechanical twin formed in the area separating a sheared micro-region and the matrix at 33% rolling reduction (ε_{VM} = 0.47): (a) bright-field image of the twin composed of segments T_1, T_2 and T_3 and embedded in the matrix M; (b), (c), (e), (f) SAD patterns obtained from the M, T_1, T_2 and T_3 regions, respectively (the corresponding locations are indicated by circles in (a)). The zone axis for the SAD patterns in (b), (c), (e) is $[1\bar{2}10]$ and for the SAD pattern in (f) this axis is $[\bar{2}4\bar{2}3]$; (d) schematic of the superimposed reciprocal lattice sections corresponding to the SAD patterns in (b) and (c) (the solid line indicates the $(10\bar{1}2)$ twinning plane).
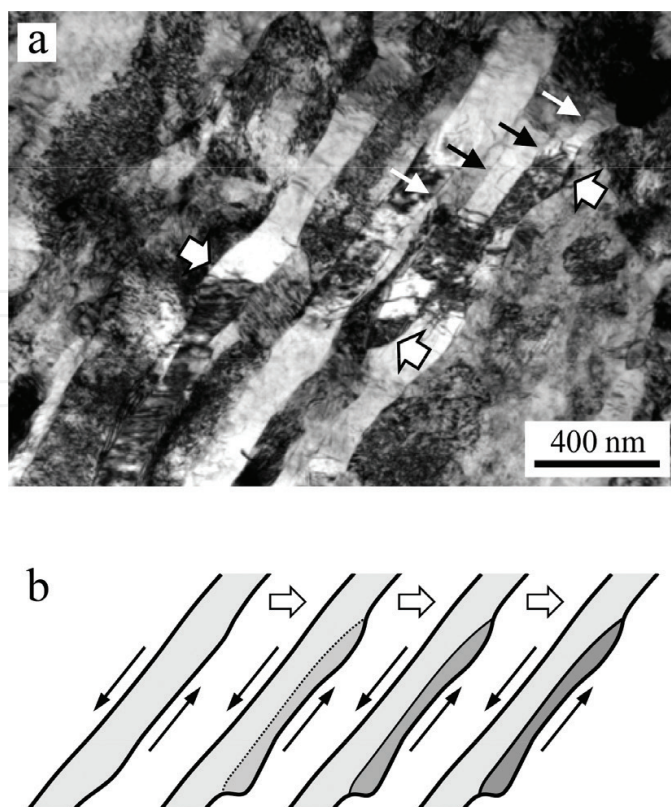
Figure 9. (a) TEM bright-field micrograph of the thin lath structure formed in a boundary region of the macroscopic shear band after 83% rolling reduction (ε_{VM} = 2.07); (b) schematic representation of the lamella longitudinal splitting process enhanced by shear induced bulging of its boundary (after ref. [10]), see text for details.

confirmed by the misorientation angle/axis pair of ~85°/ [1$\bar{2}$10] derived from the SAD patterns (see **Figure 8b** and **c**), that is consistent with that calculated for the above twin system [31, 32]. Zhu et al. [35] also observed the similar fine {10$\bar{1}$2}⟨10$\bar{1}\bar{1}$⟩ twins in the microstructure of a commercial purity Ti processed by surface mechanical attrition treatment (SMAT). The SAD patterns corresponding to the twin segments T$_1$ (**Figure 8c**) and T$_2$ (**Figure 8e**) were almost identical, which indicates that the boundary separating these segments were low-angle dis-location wall, presumably formed as a result of deformation-induced splitting of the twin lamella. By contrast, the boundary dividing segment T$_1$ and T$_3$ was a high-angle boundary, as indicated by the respective SAD patterns (**Figure 8c** and **f**), suggesting that the segment T$_3$ might originate from the part of the twin lamella formation process. A similar subdivision of mechanical twin lamellae into high-angle boundary segments was also reported in [32, 37].

In the shear-localization regions, groups of fragmented mechanical twins interspersed with the matrix, elongated lamellar structure aligned along the shear direction were frequently observed. The elongated twin/matrix lamellae in the sheared areas seem to split through the formation of dislocation walls to form a thin lath microstructure with increasing shear strain. **Figure 9a** provides the evidence for the early stages of this process observed in the boundary region of the macroscopic shear band at 83% rolling reduction. An array of parallel elongated high-angle boundary laths containing some low-angle longitudinal dislocation walls was observed (indicated by small arrows in **Figure 9a**). It is clear that the twin/matrix lamellar structure
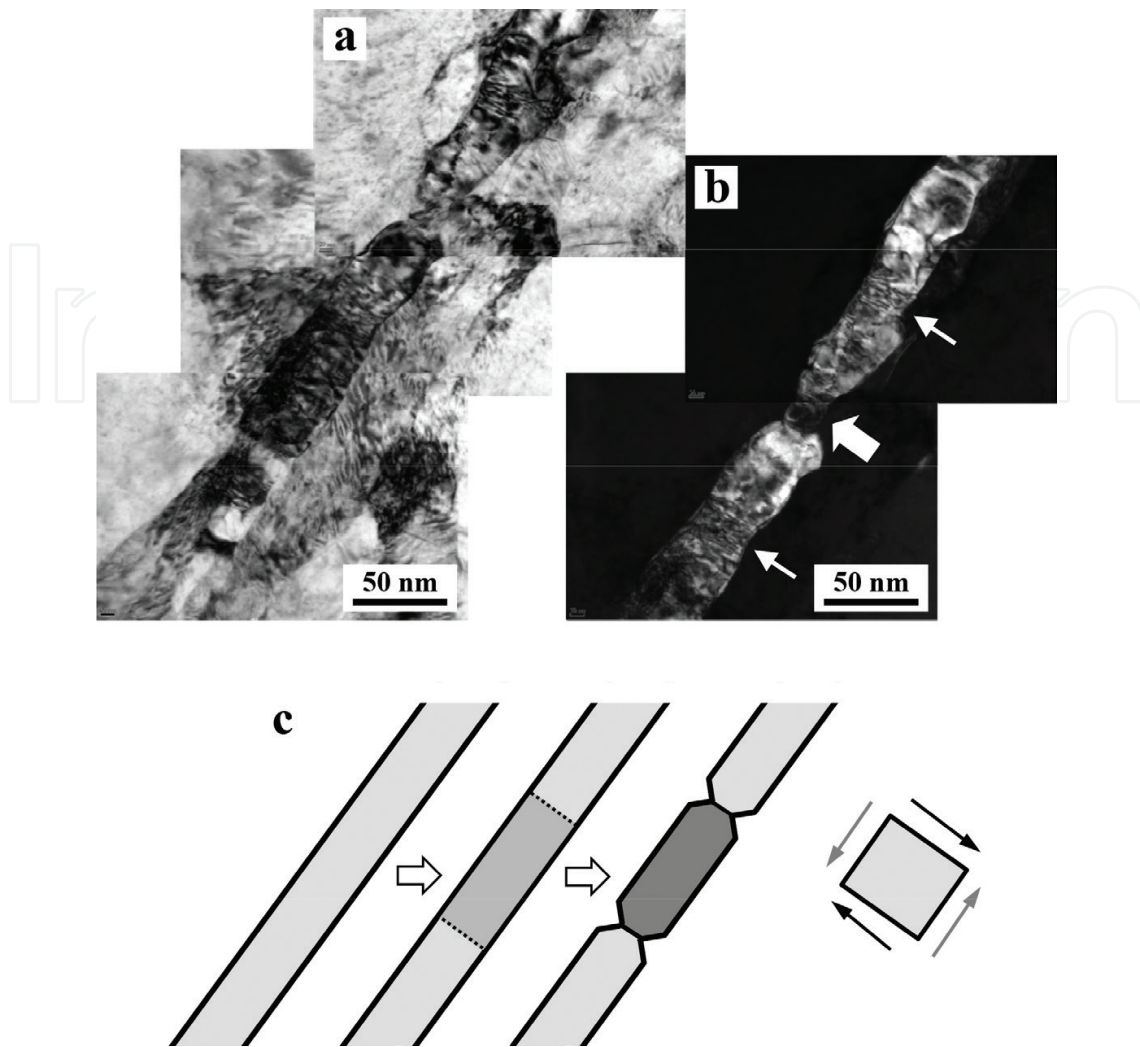
Figure 10. (a) TEM bright-field image of long laths breaking down into subgrains in a boundary region of the localized microscopic shear band after 67% rolling reduction (ε_{VM} = 1.27); (b) corresponding dark-field image; (c) schematic illustration of the breakdown process.

was progressively split and narrowed by the formation of such walls. With localized shear deformation progressing, the lath boundaries became curved and some lath regions appear to have locally been extruded out to form a bulge (marked by large arrows in **Figure 9a**). It was suggested in [10] that the bulge formation tends to accelerate the splitting process (**Figure 9b**). For a given rolling reduction, the observed range of the lath widths was generally consistent with the transverse lengths (d_T) of the fine elongated subgrains found within the shear bands. The above experimental observations thus suggest that these fine subgrains have likely formed through the deformation-induced transverse breakdown of the thin lath.

Figure 10 shows a typical long thin lath in the boundary region of a localized microscopic shear band at 67% rolling reduction. As shown, dislocations accumulated at several locations form "bamboo nodes" transverse dislocation (marked by the arrows in **Figure 10b**). The laths displayed a tendency to become constricted at the locations of the transverse boundaries (a clear example is indicated by the large arrow in **Figure 10b**). The formation of these walls

led to the lath breakdown into elongated segments. The dimensions of these segments were about 30 nm in width and 100 nm in length, which is consistent with the sizes of the elongated subgrains in the microscopic shear band. This suggests that these bamboo-node dislocation walls are precursors of the subgrains and gradually became converted to elongated subgrains having large-angle boundaries with increasing shear strain. It should be noted that the laths in **Figure 10** also clearly experienced some splitting by longitudinal boundaries except for the breakdown through the formation of transverse dislocation walls.

Figure 11 shows a lath microstructure located at the localized microscopic shear band regions at 67% rolling reduction. It contains a subgrain being in the process of its formation and thus provides an insight into the mechanism of the gradual conversion of elongated lath segments to the fine elliptical, facetted subgrains found in regions of the macroscopic shear bands. The elliptical subgrain marked 2 in **Figure 11a** has clearly been initiated from a pre-existing segment of the long thin lath labeled 1. The subgrain, with few dislocations in the interior, is separated by high-angle boundaries from the neighboring areas marked 3 and 4 (**Figure 11c–e**), originating from the highly misoriented lath interfaces. The parent lath has become markedly constricted at the boundary dividing it from the subgrain and the original facet, separating regions 2 and 4, which has split to form two new facets (**Figure 11a**). TEM observation indicated that the subgrain has undergone a significant rotation (**Figure 11b** and **c**), evidenced by that the subgrain elongation axis is slightly deflected from the long lamella axis and the subgrain remains connected to the parent lath matrix by a medium-angle boundary with a misorientation angle of about 5°. Such types of linkages between the elongated subgrains and the parent lath matrix were frequently observed in the present study. Interestingly, some roughly equiaxed fine (sub)grains were already observed within the sheared micro-regions after 33% rolling reduction (**Figure 12**). The above observations strongly suggest that the equiaxed nanosized (sub)grains found within the macroscopic shear band center at large strains (**Figure 7**) did not originate from nucleation and growth process. Instead, they likely evolve through a continuous deformation-induced fragmentation of the pre-existing thin laths, first generating fine elongated subgrains followed by the formation of equiaxed fine (sub)grains with increasing shear strain.

Figure 13 displays an example of the microstructure formed in the regions near the macroscopic shear band at 83% rolling reduction. The microstructure was rather non-uniform and contained a mix of slightly elongated and roughly equiaxed fragments that clearly formed through a process of breaking down the pre-existing elongated laths. Two clearly discernible fragmented lath segments marked by dotted lines in **Figure 13** provide a further contribution to the understanding of the earlier fragmentation process. It is also seen from **Figure 13** that the microstructure was rather "turbulent," with the laths having different longitudinal axes and displaying pronounced local bending. This likely further improved the transverse lath breakdown. Furthermore, the equiaxed fragments boundaries were sharply discernible and the dislocation density within these fragments was relatively low. Some lateral sliding and bulging of the fragments out of the parent lath matrix, which generated new boundary facets, were also frequently observed (several examples are indicated by the arrows in **Figure 13**). The extended lath boundaries largely displayed medium-to-high misorientation angles while the misorientations across the shorter transverse boundaries ranged from low to high angles. Thus, most of
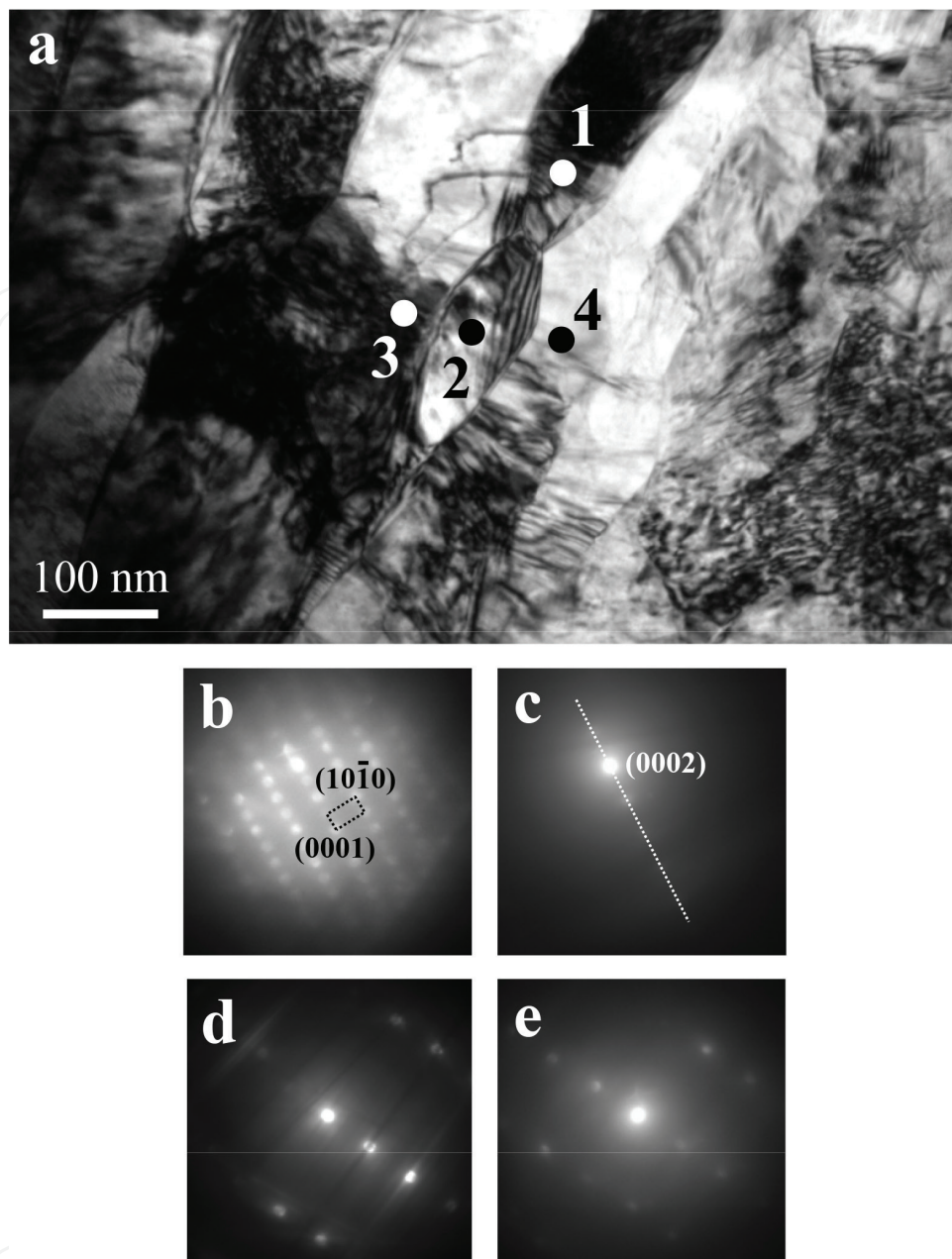
Figure 11. (a) TEM bright-field image of the thin lath structure at the boundary of the localized microscopic shear band after 67% rolling reduction (ε_{VM} = 1.27). The area contains a subgrain labeled 2 connected to the parent lath marked 1; (b-e) micro-diffraction patterns corresponding to the areas 1–4 labeled in (a), respectively. The diffraction pattern in (b) displays a [$1\bar{2}10$] zone axis and the pattern in (c) shows a systematic (0002) line of reflections (marked by the dotted line) resulting from a rotation of (b) by about 5° around the c-axis. Each of the diffraction patterns in (d) and (e) represents overlapping high-index zones and cannot be unambiguously indexed, but these patterns clearly show high-angle misorientations (above 15°) relative to (c).

the equiaxed fragments shown in **Figure 13** can be described as (sub)grains bounded partly by lower-angle and partly by high-angle boundary facets. Some of these fragments were completely bounded by high-angle boundary facets and can be thus classified as grains. The presence of polygonized, equiaxed nanosized (sub)grains, fully enclosed by high-angle boundaries, in the center, of shear bands was observed to be markedly higher than that found in the shear
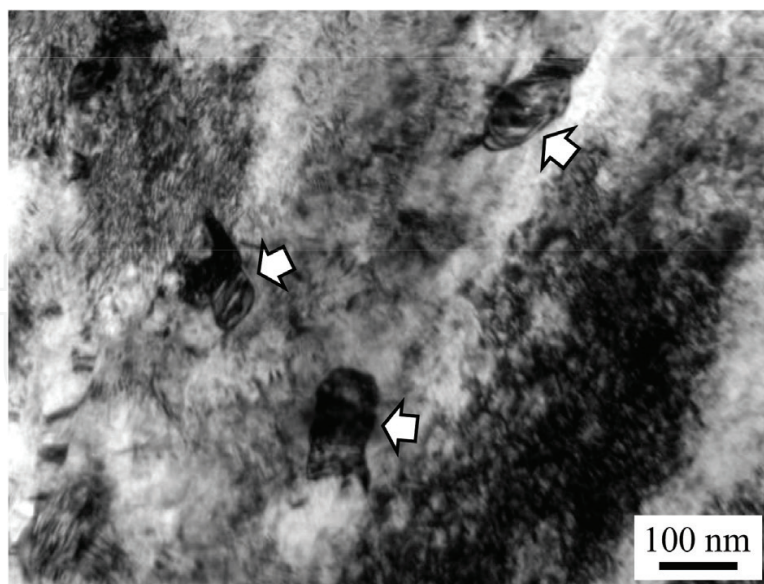
Figure 12. TEM bright-field image of the well-developed fine subgrains (arrowed) found within the sheared micro-regions after 33% rolling reduction (ε_{VM} = 0.47).
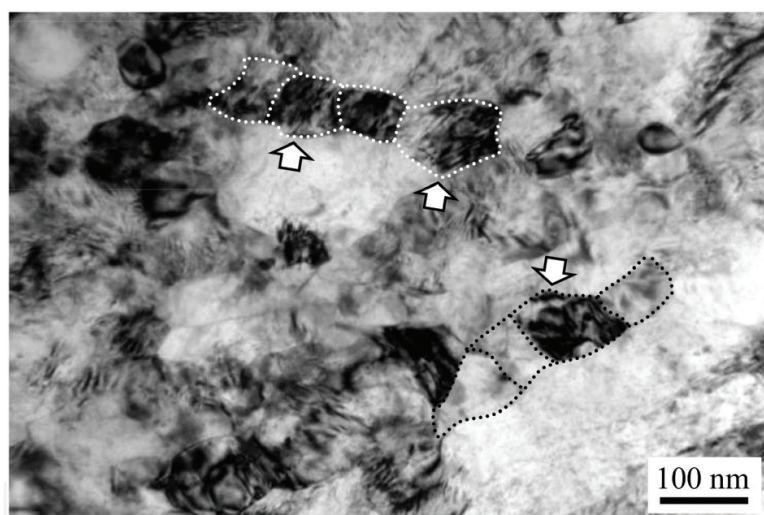

Figure 13. TEM bright-field image of the coexisting elongated subgrains and equiaxed (sub)grains in the macroscopic shear band outer region after 83% rolling reduction (ε_{VM} = 2.07).

band outer areas. This observation was likely a consequence of (sub)grain rotation promoted by a large localized shear strain developed in the shear band center, which in turn increased the frequency of high-angle boundaries compared to the outer shear band regions.

4. Discussion

The deformation-induced temperature increase plays an important role in the formation of the equiaxed fine (sub)grains inside the shear bands. Ref. [38] gives a simple calculation of the

Rolling reduction (%)	Von Mises strain ε_{VM}	Shear strain in the shear bands ε_s	Temperature increase in the matrix ΔT_M (K)	Temperature increase in the shear bands ΔT_S (K)
33	0.47	—	76	—
50	0.80	2.31	129	374
67	1.27	3.08	205	498
83	2.07	6.32	335	1020

Table 1. Estimated values of shear strain within the shear bands together with the deformation-induced temperature increases calculated for both the overall sample matrix and shear bands at different rolling reductions.

temperature increase during rolling deformation (ΔT): $\beta \sigma_{flow} \varepsilon = \rho c_p \Delta T$, where β is the thermal conversion factor taken as 0.9, σ_{flow} is the plane flow stress ($\sigma_{flow} = \frac{2}{\sqrt{3}} \times \sigma$ where σ is the tensile strength equal to 366 MPa), ε is the deformation strain, ϱ is the density equal to 4.5 g cm^{-3}, and c_p is the specific heat capacity taken as 523 J kg^{-1} K^{-1}. It is shown in **Table 1** that the temperature increase at the center of shear bands is markedly higher than that for the entire specimen. In the central region of the macroscopic shear band at 83% rolling reduction, the temperature increase estimated (~1020 K) is slightly higher than the expected recrystallization temperature of titanium [taken as 0.5 T_m, where T_m is the melting temperature of titanium (1943 K)]. However, during the rolling process, considerable specimen heat losses inevitably have occurred by both convection to the rolls and to air cooling. Therefore, the actual deformation-induced temperature increases are significantly lower than the values given in **Table 1**. This suggests that the recrystallization threshold has not likely been exceeded in the macroscopic shear band center areas, which is also supported by the absence of a microstructural feature form through the recrystallization mechanism in the shear band in our study. However, the significant temperature increases are expected to enhance the recovery processes.

The microstructure evolution within the shear localization areas can be summarized as follows. Micro-localized shear deformation regions, containing fine twin/matrix lamellae, thin laths and elongated subgrain structures interspersed with the deformed matrix, are first initiated at low strains. The formation and multiplication of approximately parallel, distinct microscopic shear bands inclined to the rolling direction at an angle of about 40° are motivated by further shear localization with increasing strain. The microscopic shear bands gradually coalesce to form a macroscopic shear band. The macroscopic shear band contains a complex structure composed of thin lath structures in the boundary regions, fine elongated subgrains in the outer areas and nanoscale, roughly equiaxed (sub)grains in the center. This suggests that the macroscopic shear band has a significant strain gradient, resulting from the band gradual development and the center region experiencing larger shear strain compared to the outer regions. The present microstructure investigation has thus clearly revealed that the above nanosized (sub)grains are formed entirely through a shear deformation-induced process. The roughly equiaxed grains in the center of shear band are a final product of the process of progressive splitting and breakdown of the thin elongated structures, which appear to partly originate from the matrix/twin lamellar structure aligned approximately parallel to the shear direction. Although there is no clear evidence of nucleation and growth of new recrystallized
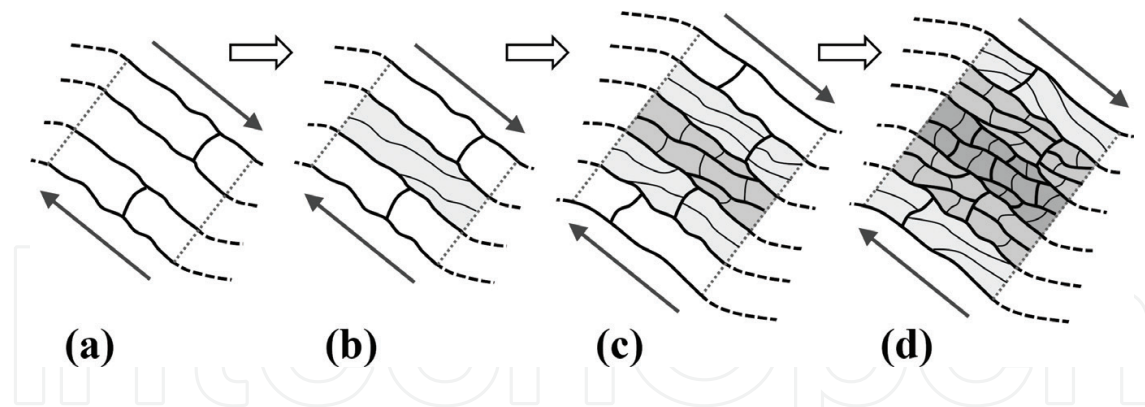
Figure 14. Schematic representation of the suggested mechanism of the microstructure evolution within the shear band interior with increasing strain: (a) formation of the mechanical twin/matrix lamellae; (b) longitudinal splitting of the lamellae to form thin laths; (c) transverse breakdown of the laths to form elongated subgrains; (d) further breakdown and rotation of the subgrains to form equiaxed nanoscale (sub)grains.

grains was observed, a deformation-induced temperature increase (**Table 1**) can be expected to enhance the recovery processes, in particular within the shear band center at large rolling reductions, which are consistent with the microstructure feature observed by TEM.

Figure 14 schematically illustrates the mechanism of the microstructure evolution within shear bands. Before the initiation of shear localization, mechanical twins are frequently observed within the deformed grains (**Figure 3**). These twins are often divided to several high-angle segments (**Figure 8**), presumably as a result of the multiple twinning events which have been reported to frequently occur within the mechanical twins formed in HCP materials [31, 32, 37]. The activation of additional twin systems is inevitably triggered by significant lattice rotation in the areas of shear localization. Then the twins are incorporated into the localized bands and gradually reorient themselves toward the shear band direction. These mechanical twins rapidly multiply until they reach a saturated state to form twin/matrix lamellar structure with a relatively narrow spacing (**Figure 14a**).

The longitudinal splitting and transverse breakdown are the two main deformation-induced processes which contribute to the gradual transition from the elongated twin/matrix lamellar structure to the final roughly equiaxed (sub)grains. The transition from the elongated twin/matrix lamellae to the thin lath structure (**Figure 14b**) is primarily achieved by longitudinal splitting mechanism. The conversion of the thin lath structure to the fine elongated subgrains is mainly controlled by the transverse breakdown mechanism (**Figure 14c** and **d**). Although longitudinal splitting generally occurs prior to intense transverse breakdown, these two mechanisms might occur simultaneously.

The mechanical twinning gradually is consumed and the dislocation activity then dominates the deformation process at large strains [35, 39]. At this stage, the progressive splitting, and narrowing, of the matrix/twin lamellae leads to the formation of finely spaced lath structure containing a mix of twin boundaries and dislocation walls (**Figure 7a**). With increasing strain, twin boundaries gradually become severely distorted and thus converted to general high-angle boundaries [40]. At same time, the dislocation walls finally become transformed to high-angle boundaries through continuing to absorb dislocations and increase their misorientations [30, 40]. As a result, it is frequently hard to clearly distinguish the origin of the lath boundaries at large strains. Ref. [10] suggested that the above splitting process is promoted by the interactions between the adjacent elongated lamellar segments under heavy shear deformation. Once the lamellae develop some perturbations or bulges, largely created due to their transverse breakdown into shorter segments,

their longitudinal boundaries become undulating (**Figure 9a** and **10**). The bulges then split from the parent lamellae driven by the adjacent segments, which result in further narrowing of the lamellae and the formation of a thin lath structure (**Figure 9b**).

The dislocations within the laths tend to accumulate at some locations to form "bamboo nodes" transverse dislocation walls. This process first leads to the formation of fine elongated subgrains through the breakdown of long lath progressive (**Figures 5, 6** and **10–12**) and finally, in conjunction with lattice rotations, to the formation of roughly equiaxed fine (sub)grains (**Figures 7** and **13**). It has been suggested that the driving force for this process is mainly provided by the conjugated shear stress [10]. This shear stress is also likely to promote the observed lateral sliding of some of the lath segments out of the parent matrix, which leads to the formation of new large-angle boundary facets (**Figures 11–13**). This mechanism is thus expected to contribute substantially to the transition from the elongated lath subgrains to the roughly equiaxed nanosized (sub)grains found in the macroscopic shear band core region (**Figure 7**). It seems plausible to expect that, with further increase in localized shear strain, the fragmentation and rotation processes within the macroscopic shear band center would ultimately lead to the formation of equiaxed nanosized grains fully enclosed by high-angle boundaries.

In the present chapter, isolated dislocations are frequently observed within both the fine elongated subgrains and ultrafine equiaxed (sub)grains. It is suggested that plastic deformation within these structures largely occurs through dislocation slip processes down to the smallest fragments observed. This is in agreement with the published data suggesting that plastic deformation was governed by the dislocation processes within microstructural fragments with 5 nm dimension [30, 40]. The gradual subdivision process of the starting matrix/twin lamellar structure of HCP titanium observed in our study within the shear localization areas might thus be principally described within the Risø framework of deformation microstructure evolution by slip processes [40], originally developed predominantly for FCC and BCC metallic materials. According to this concept, the matrix/twin lamellae tend to progressively subdivide during straining into cell blocks separated by "geometrically necessary" boundaries (GNBs) and containing "incidental" dislocation boundaries (IDBs) formed by statistical trapping of slip dislocations. Typical shapes of cell blocks accommodating large plastic strains are thin laths, delineated by extended GNBs and subdivided into shorter segments by a mix of transverse GNBs and IDBs. The lath structure parameters have been observed to scale in proportion to strain up to very large strain levels [40]. GNBs are predominantly large-angle boundaries while IDBs are generally low-angle dislocation walls at medium-to-large strains, and the misorientation angle for both the boundary types typically increases and their spacing decreases with increasing strain due to a continuous accumulation of dislocations in the structure. As a result, the GNBs are first converted into high-angle boundaries, followed by the conversion of transverse IDBs, and the grain subdivision process thus ultimately leads to the formation of nanosized equiaxed grains separated by high-angle boundaries at very large strains [40].

Terada et al. [36] reported the fine equiaxed grains of 80–100 nm in commercial purity titanium subjected to accumulated roll bonding. This mean grain size is just slightly higher than what has been achieved in the center of shear bands after 83% rolling reduction. This implies that these fine equiaxed grains might have indeed originated from macro-shear and micro-shear bands as tentatively suggested by the above authors. A considerable microstructure refinement generally associated with the adiabatic shear band development during dynamic loading was observed during the deformation by heavy cold rolling [11, 41]. The microstructure feature

observed within the shear bands produced by cold rolling appears to bear some similarity to the microstructures typically obtained by SPD processes [1, 30]. It has been suggested that intense plastic deformation within the shear band might actually be classified as an SPD process [4]. Thus, it seems plausible that some of the microstructure refinement mechanisms suggested in the present chapter might be also applicable to the SPD grain-refining processes.

5. Conclusions

This chapter presents a detailed investigation on the microstructure evolution and nanograin formation within the shear localization areas formed in commercial purity titanium during cold rolling deformation. The grain-refining mechanism has been addressed and the following conclusions can be drawn:

1. Sheared micro-regions, containing fine twin/matrix lamellae, thin laths and elongated subgrains, are first initiated at low strains and further shear localization with increasing strain leads to the formation and multiplication of distinct microscopic shear bands. The microscopic shear bands gradually coalesce to form a macroscopic shear band. The macroscopic shear band contain a mix microstructure of thin lath structures, fine elongated subgrains and roughly equiaxed (sub)grains with a mean size of about 70 nm.

2. The shear localization starts from the formation and multiplication of twin/matrix lamellar structure aligned along the shear direction. The twin/matrix lamella then splits into thin laths through the formation of longitudinal dislocation walls. The thin laths gradually transverse breakdown by the formation of short transverse dislocation boundaries. The continuing thermally assisted lath breakdown, in conjunction with lateral sliding and lattice rotations, leads to the formation of a mix of roughly equiaxed, nanosized (sub)grains and grains in the macroscopic shear band center at large strains.

3. Some of the mechanisms of the microstructure refinement within the shear localization areas suggested in the present chapter might be also applicable to other severe plastic deformation processes. The gradual microstructure fragmentation process within the shear localization areas might be principally described within the Risø framework of deformation microstructure evolution by slip processes, originally developed predominantly for FCC and BCC metallic materials.

Author details

Dengke Yang[1,2]* and Huimin Yang[3]

*Address all correspondence to: dkyang@issp.ac.cn

1 School of Materials Science and Engineering, Anhui University of Technology, Anhui, China

2 Institute for Frontier Materials, Deakin University, Victoria, Australia

3 China National Bamboo Research Center, Zhejiang, China

References

[1] Xu YB, Zhang JH, Bai YL. Shear Localization in Dynamic Deformation: Microstructural Evolution. Metallurgical and Materials Transactions A. 2008;**39A**:811

[2] Walley SM. Shear Localization: A Historical Overview. Metallurgical and Materials Transactions A: Physical Metallurgy andMaterials Science. 2007;**38A**:2629

[3] Kad BK, Gebert JM, Pérez-Prado MT, Kassner ME, Mayers MA. Ultrafine-grain-sized zirconium by dynamic deformation. Acta Materialia. 2006;**54**:4111

[4] Meyers MA, Xu YB, Xue Q, Pérez-Prado MT, McNelley TR. Microstructural evolution in adiabatic shear localization in stainless steel. Acta Materialia. 2003;**51**:1307

[5] Meyers MA, Cao BY, Nesterenko, Benson D. Xu YB. Shear localization-martensitic transformation interactions in Fe-Cr-Ni monocrystal. Metallurgical and Materials Transactions A: Physical Metallurgy and Materials Science. 2004;**35A**:2575

[6] Andrade UR, Meyers MA, Vecchio KS, Chokshi AH. Dynamic recrystallization and grain size effects in shock hardened copper. Acta Metallurgica et Materialia. 1994;**17**:175

[7] Pérez-Prado MT, Hines JA, Vecchio KS. Micmstructural evolutioninadiabaticshearband-sin TaandTa-Walloys {J}. Acta Materialia. 2001;**49**:2905

[8] Xue Q, Cerreta EK, Gray GT III. Microstructural characteristics of post-shear localization in cold-rolled 316L stainless steel. Acta Materialia. 2006;**55**:691

[9] Xue Q, Gray GT III. Development of adiabatic shear bands in annealed 316L stainless steel: Part I. Correlation between evolving microstructure and mechanical behavior. Metallurgical and Materials Transactions A: Physical Metallurgy and Materials Science. 2006;**37**:2435

[10] Xue Q, Gray GT III. Development of adiabatic shear bands in annealed 316L stainless steel: Part I. Correlation between evolving microstructure and mechanical behavior. Metallurgical and Materials Transactions A: Physical Metallurgy and Materials Science. 2006;**37**:2447

[11] Chichili DR, Ramesh KT, Hemker KJ. Adiabatic shear localization in α. Journal of the Mechanics and Physics of Solids. 2004;**52**:1889

[12] Xu YB, Bai YL, Shen LT. Formation, microstructure and development of the localized shear deformation in low-carbon steels. Acta Materialia. 1996;**44**:1917

[13] Wittman CL, Mayers MA, Pak H-r. Metallurgical Transactions A. Observation of an adiabatic shear band in AISI 4340 steel by high-voltage transmission electron microscopy. 1990;**21**:707

[14] Timothy SP, Hutchings IM. The structure or adiabatic shear bands in a titanium alloy. Acta Metallurgica. 1985;**33**:667

[15] Timothy SP. Acta Metallurgica. The structure of adiabatic shear bands in metals: A critica l review. 1987;**35**:301

[16] Wei Q, Kecskes L, Jiao T, Hartwig KT, Ramesh KT, Ma E. Adiabatic shear banding in ultra-fine-grained Fe processed by severe plastic deformation. Acta Materialia. 2004;**52**:1859

[17] Wright TW. The Physics and Mathematics of Adiabatic Shear Bands. Cambridge: Cambridge University Press; 2002

[18] Paul H, Morawiec A, Bouzy E, Fundenberger JJ, Piatkowski A. Brass-type shear bands and their influence on texture formation. Metallurgical and Materials Transactions A: Physical Metallurgy and Materials Science. 2004;**35A**:3775

[19] Dillamore IL, Roberts JG, Bush AC. Occurrence of shear bands in heavily rolled cubic metals. Metal Science. 1979;**2**:73

[20] Canova GR, Kocks UF, Stout MG. On the origin of shear bands in textured polycrystals. Scripta Metallurgica. 1984;**18**:437

[21] Lee CS, Hui WT, Duggan BJ. Macroscopic shear bands in cross-rolled α brass. Scripta Metallurgica et Materialia. 1990;**24**:757

[22] Sevillano JG, Houtte PV, Aernoudt E. The contribution of macroscopic shear bands to the rolling texture of FCC metals. Scripta Metallurgica. 1977;**11**:581

[23] Nakayama Y, Morii K. Microstructure and shear band formation in rolled single crystals of Al-Mg alloy. Acta Metallurgica. 1987;**35**:1747

[24] Embury JD, Korbel A, Raghunathan VS, Rys J. Shear band formation in cold rolled Cu-6% Al single crystals. Acta Metallurgica. 1984;**32**:1883

[25] Chowdhury SG, Das S, De PK. Cold rolling behaviour and textural evolution in AISI 316L austenitic stainless steel. Acta Materialia. 2005;**53**:3951

[26] Ohsaki S, Kato S, Tsuji N, Ohkubo T, Hono K. Bulk mechanical alloying of Cu–Ag and Cu/Zr two-phase microstructures by accumulative roll-bonding process. Acta Materialia. 2007;**55**:2885

[27] Wei Q, Jia D, Ramesh KT, Ma E. Evolution and microstructure of shear bands in nano-structured Fe. Applied Physics Letters. 2002;**81**:1240

[28] Cizek P, Bai F, Rainforth WM, Beynon JH. Fine structure of shear bands formed during hot deformation of two austenitic steels. Materials Transactions. 2004;**45**:2157

[29] Cizek P. Electron backscatter diffraction (ebsd) – The Method and its applications in materials science and engineering. Materials Science and Engineering A. 2002;**324**:214

[30] Lu K, Hansen N. Structural refinement and deformation mechanisms in nanostructured metals. Scripta Materialia. 2009;**60**:1033

[31] Chun YB, Yu SH, Semiatin SL, Hwang SK. Effect of deformation twinning on micro-structure and texture evolution during cold rolling of CP-titanium. Materials Science and Engineering A. 2005;**398**:209

[32] Stanford N, Carlson U, Barnett MR. Deformation Twinning and the Hall–Petch Relation in Commercial Purity Ti Metallurgical and Materials Transactions A: Physical Metallurgy and Materials Science. 2008;**39A**:934

[33] Lutjering G, Williams JC. Titanium. Engineering Materials and Processes. New York: Springer; 2003

[34] Shin DH, Kim I, Kim J, Kim YS, Semiatin SL. Microstructure development during equal-channel angular pressing of titanium. Acta Mater. 2003;**51**:983-996

[35] Zhu KY, Vassel A, Brisset F, et al. Nanostructure formation mechanism of α-titanium using SMAT [J]. Acta Mater. 2004;**52**(14):4101-4110

[36] Terada D, Inoue S, Tsuji N. Microstructure and mechanical properties of commercial purity titanium severely deformed by ARB process. Journal of Materials Science. 2007;**42**:1673

[37] Cizek P, Barnett MR. Characteristics of the contraction twins formed close to the fracture surface in Mg–3Al–1Zn alloy deformed in tension. Scripta Materialia. 2008;**59**:959

[38] Jiang L, Pérez-Prado MT, Gruber PA, Arzt E, Ruano OA, Kassner ME. Microstructure and mechanical properties of equiaxed ultrafine-grained Zr fabricated by accumulative roll bonding. Acta Materialia. 2008;**56**:1228

[39] Hughes DA, Hansen N. Deformation structure developing on fine scales. Philosophical Magazine. 2003;**83**:3871

[40] Hansen N. Metallurgical and Materials Transactions A. New discoveries in deformed metals. 2001;**32A**:2917

[41] Meyers MA, Subahash G, Kad BK, Prasad L. Mechanics of Materials. Evolution of Microstructure and Shear-Band Formation in a-hcp Titanium. Mechanics of Materials. 1994;**17**:175